Inorganic Chemistry

Article

pubs.acs.org/IC

Pyrazinoporphyrazines with Externally Appended Pyridine Rings. 13. Structure, UV−Visible Spectral Features, and Noncovalent Interaction with DNA of a Positively Charged Binuclear (Zn^{II}/Pt^{II}) Macrocycle with Multimodal Anticancer Potentialities

Ilse Manet,*[,†] Francesco Manoli,[†] Maria Pia Donzello,*[,‡] Elisa Viola,[‡] Annalisa Masi,[§] Giuseppina Andreano,[§] Giampaolo Ricciardi,[∥] Angela Rosa,[∥] Luciano Cellai,[§] Claudio Ercolani,[‡] and Sandra Monti[†]

[†]Istituto per la Sintesi Organica e la Fotoreattività, Consiglio Nazionale delle Ricerche, via Gobetti 101, I-40129 Bologna, Italy

[‡]Dipartimento di Chimica, Università "La Sapienza", P.le A. Moro 5, I-00185 Roma, Italy

[§]Istituto di Cristallografia, Consiglio Nazionale delle Ricerche, Area della Ricerca di Roma 1, 00015 Monterotondo Scalo, Rome, Italy

[∥]Dipartimento di Scienze, Università della Basilicata, Viale dell'Ateneo Lucano 10, I-85100, Potenza, Italy

Supporting Information

ABSTRACT: We investigated with spectroscopic techniques the noncovalent interaction of a bimetallic water-soluble (Zn^{II}/Pt^{II}) porphyrazine hexacation, $[(PtCl_2)(CH_3)_6LZn]^{6+}$, and its octacationic analogue $[(CH_3)_8LZn]^{8+}$, lacking the *cis*-platin-like functionality, with a 21-mer double strand (ds) 5′-d[GGG(TTAGGG)$_3$]-3′/3′-d[CCC(AATCCC)$_3$]-5′, as model for B-DNA. Both hexacation and octacation tend to aggregate in water. The structure as well as the ground and excited-state electronic properties of the Zn^{II}/Pt^{II} hexacation $[(PtCl_2)(CH_3)_6LZn]^{6+}$ in water solution were investigated using density functional theory (DFT) and time-dependent DFT (TDDFT) methods. TDDFT calculations of the lowest excited states of $[(PtCl_2)(CH_3)_6LZn]^{6+}$ in water provided an accurate description of the Q-band spectral region. In particular, the calculated optical spectra were in agreement with the experimental ones, obtained in the presence of micelles favoring complete disruption of the aggregates. The model for dsDNA binding that emerges from the analysis of UV−vis absorption and time-resolved fluorescence data shows the presence of complexes of 1 dsDNA molecule with 1, 2, and 4 macrocycles. Comparing the results for the hexacation $[(PtCl_2)(CH_3)_6LZn]^{6+}$ with those for the $[(CH_3)_8LZn]^{8+}$octacation, we observed a higher degree of monomerization for the $[(PtCl_2)(CH_3)_6LZn]^{6+}$ derivative.

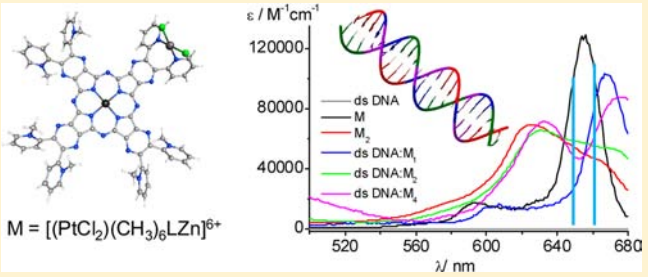

INTRODUCTION

Multimodal therapy based on the synergic action of different drugs or treatments is commonly used to combat various diseases including cancer.[1] However, the combination of different drugs or treatments has to occur with an intricate balance of dosage and timing to guarantee the positive therapeutic outcome. A lot of efforts are nowadays concentrated on the design of single therapeutic agents allowing one to implement multiple treatment modalities.[2] In this frame, we reported recently on the synthesis of a water-soluble Zn(II) pyrazinoporphyrazine hexacation, $[(PtCl_2)(CH_3)_6LZn]^{6+}$, bearing an exocyclic $N_{2(pyr)}PtCl_2$ coordination site (Figure 1A).[3] We showed that this Zn^{II}/Pt^{II} hexacation behaves as an efficient photosensitizer in DMF solution generating singlet oxygen, $^1O_2$, a highly cytotoxic species.[3] The very good quantum yield of $^1O_2$ production ($\Phi_\Delta = 0.46$) makes it an interesting agent for application in photodynamic therapy (PDT).[4] The hexacation also proved to interact with the single-stranded telomeric DNA guanine-rich sequence 5′-d[AGGG(TTAGGG)$_3$]-3′, present as a G-quadruplex-type structure (G4) in K^+ or Na^+ 0.1 M water solutions.[5] The binding of the hexacation influences the conformational equilibrium of the G4 structure in 0.1 M K^+ solution, yielding very stable complexes with G4 mainly in parallel conformation. This observation represents a second important outcome for the present heterobimetallic cation as potential agent for multimodal anticancer therapy. In fact, ligands that bind in solution to G-quadruplex DNA, stabilizing the structure, can also interfere with the biological processes involving guanine-rich sequences, present both in telomeres and in promoter regions of some oncogenes.[6,7] With these biological processes being crucial for cancer cell survival and replication, guanine-rich sequences have become a very promising target for the development of new anticancer

Received: September 25, 2012
Published: December 17, 2012

dx.doi.org/10.1021/ic3020755 | *Inorg. Chem.* 2013, 52, 321−328

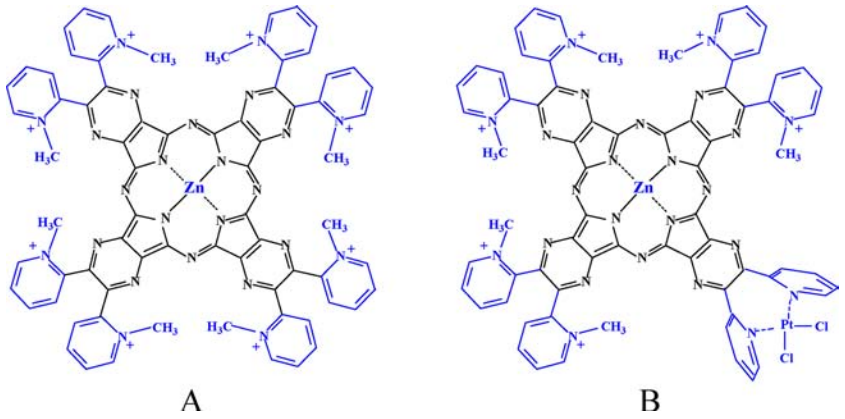

Figure 1. (A) The hexacation $[(PtCl_2)(CH_3)_6LZn]^{6+}$; (B) the octacation $[(CH_3)_8LZn]^{8+}$ (L = tetrakis-2,3-[5,6-di(2-pyridyl)pyrazino]-porphyrazinato dianion). Both cationic porphyrazines are neutralized by I^- ions.[3,10]

drugs and attracted a lot of research interest during the past decade.[7,8]

Furthermore, the exocyclic $N_{2(pyr)}PtCl_2$ coordination site in $[(PtCl_2)(CH_3)_6LZn]^{6+}$ (Figure 1A) closely resembles cis-platin, $(NH_3)_2PtCl_2$, an extensively used chemotherapeutic anticancer drug.[9] Because the presence of the *cis*-platin-like functionality for the hexacation $[(PtCl_2)(CH_3)_6LZn]^{6+}$ might represent a third potential cancer treatment modality, we investigated the noncovalent interaction of the Zn^{II}/Pt^{II} hexacation with the 21-mer double-strand (ds) 5′-d[GGG-(TTAGGG)$_3$]-3′/3′-d[CCC(AATCCC)$_3$]-5′, as model for B-DNA. For comparison, a parallel investigation was carried out for the related octacation $[(CH_3)_8LZn]^{8+}$ lacking the *cis*-Pt functionality (Figure 1B). The study of the binding was performed monitoring absorption, fluorescence, and circular dichroism (CD) and was accompanied by the theoretical investigation of structural features and optical absorption properties of the Zn^{II}/Pt^{II} hexacation, useful for an understanding of the solution spectra of this molecule. The overall findings allow one to envisage for the hexacation three-modal therapeutic anticancer potentialities.

EXPERIMENTAL AND COMPUTATIONAL SECTION

The charged macrocycles $[(PtCl_2)(CH_3)_6LZn]^{6+}$ and $[(CH_3)_8LZn]^{8+}$ in the form of the iodide salt-like species were prepared as reported previously.[3,10] The possible presence of impurities due to incomplete quaternization and/or multiple platination in the sample is not believed to be significant.[3,10] The telomeric sequence 5′-d[GGG-(TTAGGG)$_3$]-3′ (21-mer) and its complementary strand were prepared by automated synthesis according to standard procedures.

Quantum Chemical Calculations on the Hexacation $[(PtCl_2)(CH_3)_6LZn]^{6+}$. Density functional theory (DFT) and time-dependent DFT (TDDFT) calculations were performed with the Amsterdam Density Functional (ADF) program package, release 2012.01,[11,12] employing the scalar relativistic zeroth-order regular approximation (ZORA) formalism[13] and the all-electron ZORA/TZP basis set.[14] The ground-state molecular structure of $[(PtCl_2)(CH_3)_6LZn]^{6+}$ was fully optimized (without constraints) in water solution (ε = 78.39) using the BP86[15] exchange-correlation functional. The optimized structure was verified to be a true minimum by frequency calculations. The vertical absorption energies and oscillator strengths of the lowest singlet excited states were computed at TDDFT level using the hybrid B3LYP[16] functional. Solvation effects on the ground-state molecular and electronic structure and on the excited states were modeled through a dielectric continuum model, which was chosen to be the COSMO model.[17] The calculated excitation energies contain, apart from the altered "solvated" orbitals (slow term), also the contributions from the "fast" solvent response term.[18]

Sample Preparation for Solution Studies. The buffer for the spectroscopic measurements contained 10 mM Tris and 100 mM KCl. Excess of K^+ mimics physiological conditions of cellular compartments where K^+ is abundant. pH was corrected to a value of 7.4 with aliquots of HCl 3 N. Solutions of the two complementary single strand sequences were prepared, and the concentrations were determined spectrophotometrically. Equimolar aliquots of both solutions were mixed and heated at 90 °C for 15 min and then cooled to room temperature before use. The iodide salt of $[(PtCl_2)(CH_3)_6LZn]^{6+}$ was dissolved up to a concentration of 1.2×10^{-5} M in the buffer. Aliquots of the charged macrocycle solution and of DNA duplex solution in the same buffer were mixed to obtain the desired molar ratio. Water was purified by passage through a Millipore Milli-Q system (Millipore SpA, Milan, Italy).

Photophysical Measurements. UV−visible absorption spectra were recorded on a Perkin-Elmer λ 650 spectrophotometer. Fluorescence spectra were obtained on a Spex Fluorolog 111A spectrofluorimeter. Right angle detection was used. CD spectra were obtained with a Jasco J-715 spectropolarimeter. Each CD spectrum was registered accumulating 4 scans with integration time of 1 s; scan rate was 50 nm/min for the whole nm range. All of the measurements were carried out at 295 K in quartz cuvets with path length of 2.0 cm and 0.5 and 0.2 cm for the UVB.

Titration experiments with detection of absorption, CD, and fluorescence were performed at constant ligand and varying duplex DNA concentrations. The best complexation model and the related association constants were determined by global analysis of multi-wavelength data sets corresponding to 10 absorption spectra of different mixtures in the 500−680 nm range, using the commercially available program SPECFIT/32 (version 3.0.40, TgK Scientific).[19] The multivariate optimization procedure is based on singular value decomposition (SVD) and non linear regression modeling by the Levenberg−Marquardt algorithm. The deviations of the calculated absorbance from the experimental values were minimized in a completely numerical procedure. See the Supporting Information for further details.

Fluorescence lifetimes were measured in air-equilibrated solutions with a time correlated single photon counting system (IBH Consultants Ltd.). A nanosecond LED source at 373 nm was used for excitation, and the emission was collected at right angle at 670 nm using a long pass cutoff filter at 645 nm. The software package for the analysis of the emission decays was provided by IBH Consultants Ltd. Decay profiles were fitted using a multiexponential function and deconvolution of the instrumental response.

$$I(t) = \Sigma_i a_i \times \exp(-t/\tau_i) \quad (1)$$

$$f_i = (a_i \times \tau_i)/\Sigma_j(a_j \times \tau_j) \quad (2)$$

dx.doi.org/10.1021/ic3020755 | *Inorg. Chem.* 2013, 52, 321−328

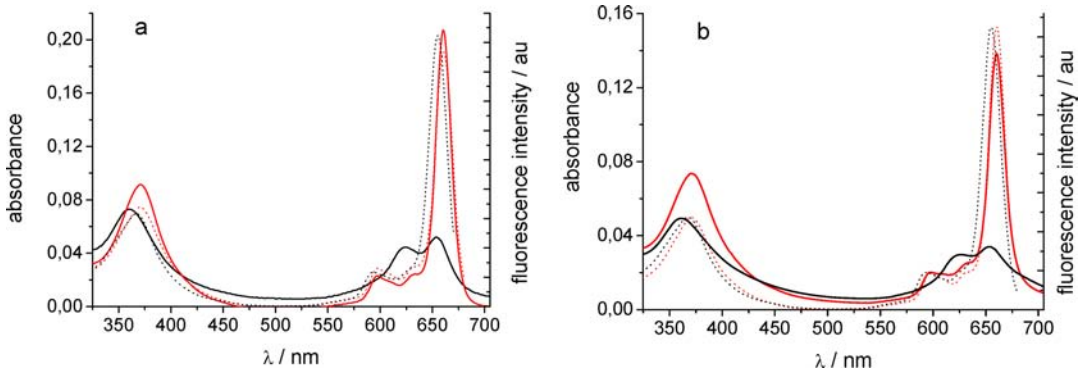

Figure 2. Absorption (line) and corrected fluorescence excitation (dotted) spectra of 1×10^{-6} M solutions of $[(PtCl_2)(CH_3)_6LZn]^{6+}$ (a) and $[(CH_3)_8LZn]^{8+}$ (b) in pure water (black) and in water with 20 mM SDS (red); d = 1.0 cm, 22 °C. Excitation spectra were measured at emission wavelength of 690 nm for solutions absorbing less than 0.1 in the explored range.

Global analysis of the decay profiles was performed for the porphyrazines in the presence of three different concentrations of DNA.

RESULTS AND DISCUSSION

Structure and UV−Visible Absorption Properties. The hexacationic Zn^{II}/Pt^{II} macrocycle, $[(PtCl_2)(CH_3)_6LZn]^{6+}$, and its related octacation, $[(CH_3)_8LZn]^{8+}$, exhibit in organic aprotic solvents (DMSO, pyridine, and DMF) a UV−visible spectrum characterized by a narrow sharp Q-band at ca. 665 nm expected for a monomeric species. Both charged species show moderate solubility in water, and in this medium they show two intense absorptions in the Q-band region with maxima of comparable intensity at ca. 625 and ca. 655 nm attributable, as was widely illustrated before,[5,10,20] to the presence of a dimer−monomer equilibrium, with the peak at lower energy (655 nm) assigned to the monomeric species. In Figure 2 the absorption spectra of the porphyrazines in pure water are compared to those recorded in the presence of sodium dodecylsulfate (SDS) micelles. The latter spectra (λ_{max} = 660 nm) clearly indicate that the dimer−monomer equilibrium is completely shifted toward the formation of the monomer (λ_{max} = 665 nm), due most likely to association of both macrocycles to the negatively charged micelle surface. Because the absorption spectrum of the monomeric species is crucial for the interpretation of the absorption titration data of the present work, we further support the relationship between structural and optical properties for the monomeric hexacation $[(PtCl_2)(CH_3)_6LZn]^{6+}$ with accurate DFT and TDDFT calculations.

Unconstrained geometry optimization of the heterobimetallic hexacationic complex in water solution afforded the C_1 symmetry structure displayed in Figure 3. $[(PtCl_2)(CH_3)_6LZn]^{6+}$ is characterized by a nearly planar Zn(II) pyrazinoporphyrazine macrocycle with a mean value of the Zn−N_p (N_p = pyrrolic nitrogen) of 2.0131 Å. The appended N-methylated pyridine rings are tilted with respect to the pertinent pyrazine ring by ∼57°, with the vicinal methyl groups (the methyl substituents residing on the same pyrazine subunit) assuming a *ud* (*u* = up; *d* = down) orientation. Structures with a *uu* or *dd* orientation of the vicinal methyl groups were also theoretically explored and resulted less stable than the C_1 structure of Figure 3. In the exocyclic $N_{2(pyr)}PtCl_2$ coordination site, the metal center displays a slightly distorted square-planar geometry with mean Pt−N and Pt−Cl bond lengths of 2.034 and 2.340 Å, respectively. The $PtCl_2$ unit is slightly bent toward the macrocycle with a dihedral angle between the pyrazine ring and the plane through the N_2PtCl_2 unit of 84.6°. The pyridine rings coordinated to the Pt(II) center assume a nearly orthogonal orientation, forming a dihedral angle of 84.6°. The structural parameters theoretically predicted for the exocyclic $N_{2(pyr)}PtCl_2$ coordination site in $[(PtCl_2)(CH_3)_6LZn]^{6+}$ are very similar to those found in the X-ray structure of $[(CN)_2Py_2PyzPtCl_2]$.[21]

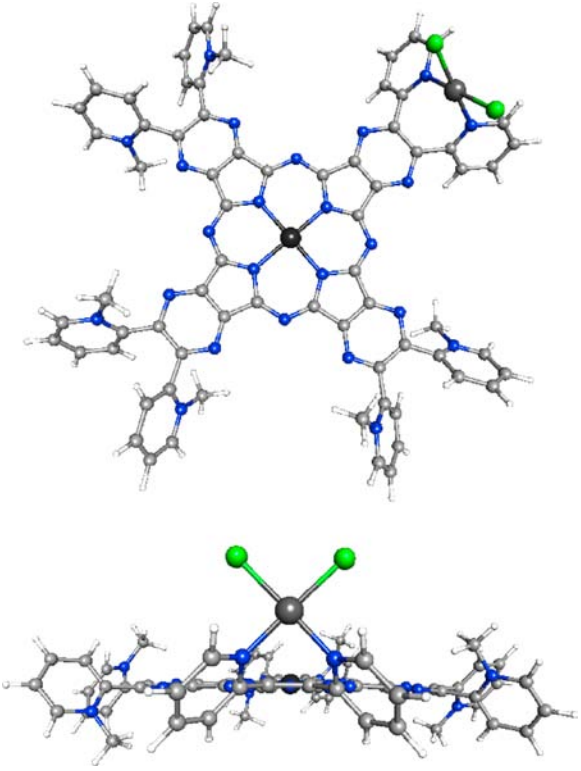

Figure 3. Top and edge-on views of the DFT-ZORA/BP86/COSMO-optimized structure of $[(PtCl_2)(CH_3)_6LZn]^{6+}$ in water solution.

The highest occupied and lowest unoccupied ground-state one-electron levels computed for the water solvated hexacationic complex are shown in Figure 4a. The HOMO and the two nearly degenerate LUMOs are basically π MOs of the pyrazinoporphyrazine macrocycle, as apparent from the plots of these orbitals also displayed in Figure 4a. Notably, in these MOs one may recognize the well-known Gouterman MOs of *Pcs* (*Pc* = phthalocyanine), with the contribution of the C_{ortho}-$2p_z$ of the benzo rings being replaced by the N_{pyz}-$2p_z$ of the

dx.doi.org/10.1021/ic3020755 | *Inorg. Chem.* 2013, 52, 321−328

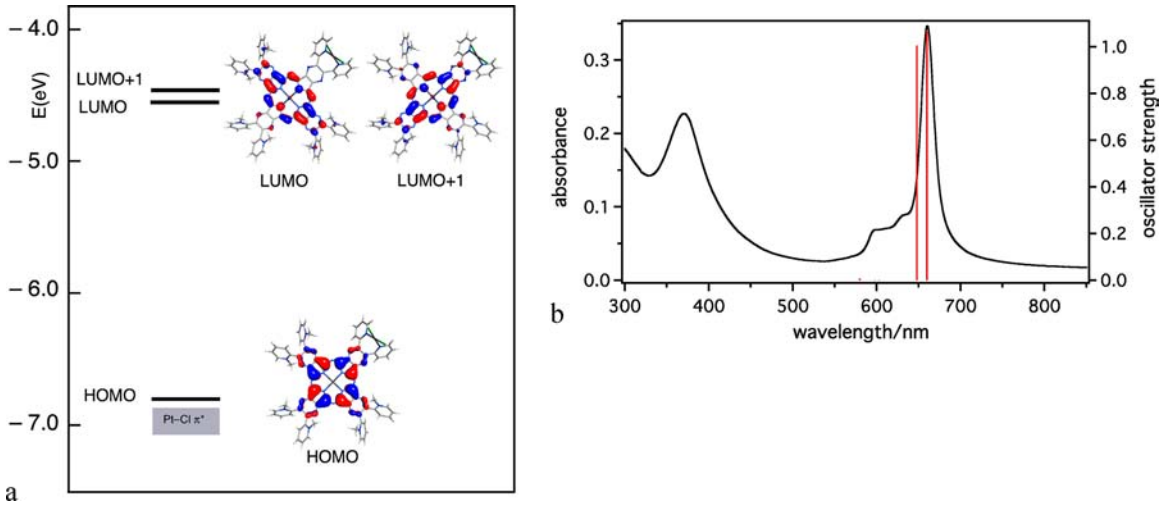

Figure 4. (a) DFT-ZORA/B3LYP/COSMO frontier orbitals of $[(PtCl_2)(CH_3)_6LZn]^{6+}$ in water solution. Also shown are isodensity surface plots of the Gouterman MOs. (b) The excitation energies and oscillator strengths computed for the lowest excited states of $[(PtCl_2)(CH_3)_6LZn]^{6+}$ in water solution are compared to the experimental (this work) absorption spectrum of the complex in water/SDS solution.

pyrazine rings. Immediately below the HOMO, there is a set of four MOs with Pt−Cl π-antibonding character.

The excitation energies and oscillator strengths calculated for the singlet excited states of $[(PtCl_2)(CH_3)_6LZn]^{6+}$ up to 450 nm, in water solution, indicate that in the Q-band region there are only two intense, close-lying, excited states, the 1^1A and 2^1A, originating from the HOMO→LUMO and HOMO→LUMO+1 transitions, respectively. These states, computed at 660 and 648 nm and with oscillator strength of 1.064 and 1.020, unambiguously account for the Q(0,0) band peaking at 660 nm in the UV−vis spectrum of the hexacationic complex taken in water/SDS solution (see Figure 4b). In the spectral range 650−450 nm, TDDFT calculations predict eight extremely weak excited states involving transitions from the set of Pt−Cl π-antibonding MOs into the LUMO and LUMO +1.

Solution Studies. In the present study, all of the spectroscopic titrations in water solution were performed keeping the porphyrazine concentration constant. To properly analyze the spectroscopic data, the self-association behavior of $[(PtCl_2)(CH_3)_6LZn]^{6+}$ and $[(CH_3)_8LZn]^{8+}$ in aqueous solution has been investigated. As we have mentioned above, this process mainly relies on the formation of dimers that are disrupted in SDS micellar medium (see Figure 2). In the hypothesis that in the presence of SDS the monomerization is complete, we calculated the molar absorption coefficient for the monomer of both macrocycles at its peak wavelength, $\varepsilon(\lambda_{max})$. The obtained values of 1.4×10^5 and 2.1×10^5 M^{-1} cm^{-1} for $[(PtCl_2)(CH_3)_6LZn]^{6+}$ and $[(CH_3)_8LZn]^{8+}$, respectively, are in excellent agreement with the corresponding values in organic solvents.[3,20] Figure 2 also reports the corrected fluorescence excitation spectra measured at λ_{em} = 690 nm in the presence of SDS micelles. They are similar to the absorption spectra and indicate the emission comes from monomeric $[(PtCl_2)(CH_3)_6LZn]^{6+}$ and $[(CH_3)_8LZn]^{8+}$. The corrected fluorescence excitation spectra of the macrocyles alone in pure water assume the same morphology as those in the presence of SDS, apart from a slight red shift of 5 nm in the latter, due to the interaction with the micellar surface. We reasonably conclude that the steady-state emission of $[(PtCl_2)(CH_3)_6LZn]^{6+}$ and $[(CH_3)_8LZn]^{8+}$ in pure water is mainly due to their monomeric species. We used the excitation spectra in the 500−680 nm range to calculate the molar absorption coefficient $\varepsilon(\lambda)$ of the monomers in water and used this information as constraint to analyze the concentration dependence of the absorption spectra of the macrocycles in water (see paragraph S1 in the Supporting Information for more details). Dimerization constants (K_d/M^{-1}) with log value of 6.99 ± 0.02 for $[(PtCl_2)(CH_3)_6LZn]^{6+}$ and 7.12 ± 0.04 for $[(CH_3)_8LZn]^{8+}$ were determined. In Figure 5c and d, the spectra for the monomer and dimer of both macrocycles are reported. The present log K_d values represent a revision of the previously reported values of 5.8 and 6.6 for $[(PtCl_2)(CH_3)_6LZn]^{6+}$ and $[(CH_3)_8LZn]^{8+}$, respectively.[5,20] Actually, the former analysis of the dimerization equilibria did not include the monomer spectra as constraints, so lower dimerization constants and different spectra for the monomeric and dimeric species were obtained. We are confident that the present analysis has higher reliability because the spectrum assigned to the monomer in water is very similar to that in organic solvents and in aqueous SDS solution and is further supported by the TDDFT calculations.

With the information on the dimerization equilibria in water, we were able to interpret the absorption spectra for titration of both $[(PtCl_2)(CH_3)_6LZn]^{6+}$ and $[(CH_3)_8LZn]^{8+}$ with ds 21-mer, shown in Figure 5a and b. At first inspection, the spectral changes indicate that association to dsDNA induces monomerization of $[(PtCl_2)(CH_3)_6LZn]^{6+}$, whereas it maintains $[(CH_3)_8LZn]^{8+}$ in dimeric form.[3] We globally analyzed each set of spectra with a binding model involving three DNA complexes; we introduced the porphyrazine monomer−dimer equilibrium in the calculations with fixed constant and fixed absorption spectra of monomeric and dimeric species; we also fixed the absorption spectrum of the 1:1 complex.

The latter was obtained from the qualitative profile of the fluorescence excitation spectrum taken at λ_{em} = 690 nm in a solution of $[(PtCl_2)(CH_3)_6LZn]^{6+}$ or $[CH_3)_8LZn]^{8+}$ in the presence of an excess of dsDNA; this profile (see inset in Figure 5a and b) clearly shows that a monomeric ligand is responsible for the emission in the complexed form. We attributed to the complexed monomer the absolute molar absorption coefficients of the free monomer, corrected for the larger width of the

dx.doi.org/10.1021/ic3020755 | Inorg. Chem. 2013, 52, 321−328

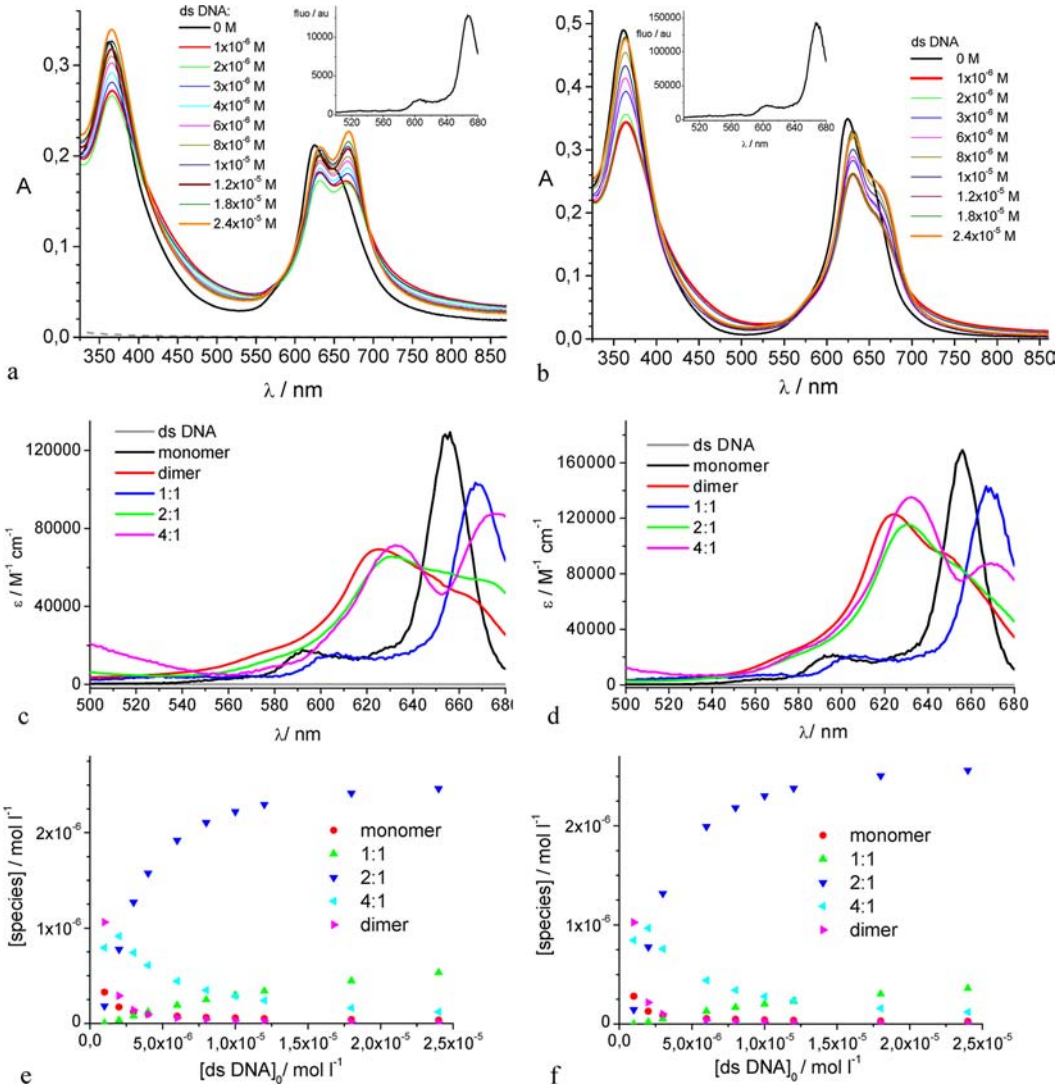

Figure 5. (a) Absorption spectra of a 6×10^{-6} M $[(PtCl_2)(CH_3)_6LZn]^{6+}$ solution with increasing dsDNA concentration (range 0.1−2.4) $\times 10^{-5}$ M in Tris 10 mM buffer, 0.1 M KCl, pH 7.4, d = 1.0 cm, 22 °C. (b) Absorption spectra of a 6.0×10^{-6} M $[(CH_3)_8LZn]^{8+}$ solution with increasing dsDNA concentration (range 0.1−2.4) $\times 10^{-5}$ M in Tris 10 mM buffer, 0.1 M KCl, pH 7.4, d = 1.0 cm, 22 °C. Note: Absorption spectra of $[(PtCl_2)(CH_3)_6LZn]^{6+}$ and $[(CH_3)_8LZn]^{8+}$ alone are in black. Inset shows the corrected excitation spectrum measured at 690 nm of $[(PtCl_2)(CH_3)_6LZn]^{6+}$ and $[(CH_3)_8LZn]^{8+}$ in the presence of a 4-fold excess of DNA. (c) Calculated absorption spectra (ε) in correspondence of the Q-band of monomeric and dimeric $[(PtCl_2)(CH_3)_6LZn]^{6+}$ and the hexacation:dsDNA complexes, $\log(K_{11}/M^{-1}) = 5.85 \pm 0.03$, $\log(K_{21}/M^{-2}) = 13.96 \pm 0.05$, and $\log(K_{41}/M^{-4}) = 27.53 \pm 0.15$. (d) Calculated absorption spectra (ε) of monomeric and dimeric $[(CH_3)_8LZn]^{8+}$ and the octacation:dsDNA complexes, $\log(K_{11}/M^{-1}) = 5.84 \pm 0.08$, $\log(K_{21}/M^{-2}) = 14.30 \pm 0.14$, and $\log(K_{41}/M^{-4}) = 28.18 \pm 0.35$.

complex emission band (we adopted a Gaussian profile). With the mentioned constraints, the global fitting afforded stoichiometry, binding constants, and individual absorption spectra of the other DNA complexes (see S2 of the Supporting Information for more information). The experimental data of Figure 5a were best reproduced with complexes of 1:1, 2:1, and 4:1 $[(PtCl_2)(CH_3)_6LZn]^{6+}$:dsDNA stoichiometry, in equilibrium with the free components. The optimized binding constants were $\log(K_{11}/M^{-1}) = 5.85 \pm 0.03$, $\log(K_{21}/M^{-2}) = 13.96 \pm 0.05$, and $\log(K_{41}/M^{-4}) = 27.53 \pm 0.15$. For $[(CH_3)_8LZn]^{8+}$, the data in Figure 5b were best reproduced with the same complexation model, and the optimized binding constants were $\log(K_{11}/M^{-1}) = 5.84 \pm 0.08$, $\log(K_{21}/M^{-2}) = 14.30 \pm 0.14$, and $\log(K_{41}/M^{-4}) = 28.18 \pm 0.35$. The formation of complexes with only three types of stoichiometry may be a simplified representation of the binding equilibria in the system; however, the global fitting did not attain convergence with any other binding model. Thus, we are confident our analysis enlightened the main features of the complexation process.

Comparing the results for $[(PtCl_2)(CH_3)_6LZn]^{6+}$ and $[(CH_3)_8LZn]^{8+}$, one can notice both similarities and differences. The binding constants are of the same order in both systems; the spectra of the complexed species (Figure 5c and d) exhibit a typical red shift as well as a hypochromic effect as compared to those of the free ligands; the absorption profiles of the 1:1 and 2:1 complexes are similar in both compounds; on the contrary, the absorption spectrum of the 4:1 complex is different, showing in the case of $[(PtCl_2)(CH_3)_6LZn]^{6+}$ a more intense peak at the red side of the Q-band. Likely in the 4:1 complexes, the macrocyle is associated both as dimer and as monomer at different sites of the dsDNA, and the relative weight of the two forms is different for the two compounds, with the monomeric form favored over the dimeric form in the 4:1 complex of the

dx.doi.org/10.1021/ic3020755 | Inorg. Chem. 2013, 52, 321−328

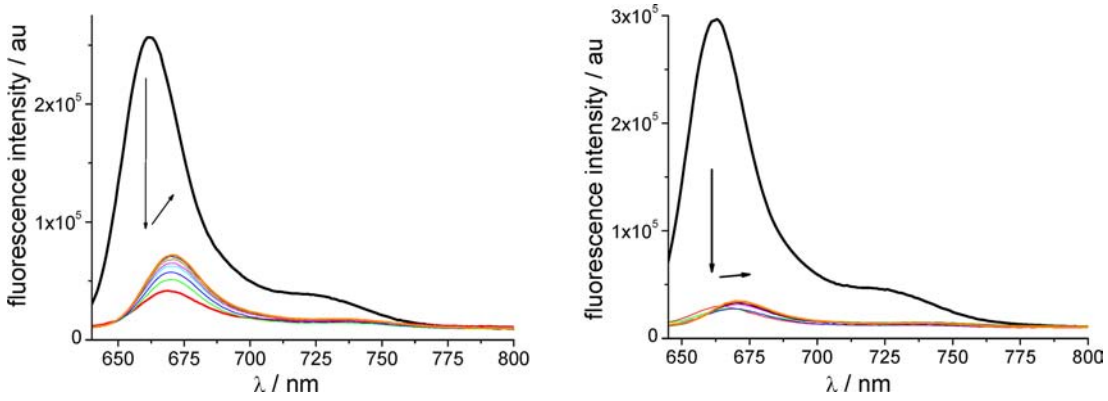

Figure 6. Titration of a 6×10^{-6} M $[(PtCl_2)(CH_3)_6LZn]^{6+}$ (left) or $[(CH_3)_8LZn]^{8+}$ (right) solution with increasing dsDNA concentration (range 0.06–2) $\times 10^{-5}$ M in Tris 10 mM buffer with KCl 0.1 M, pH 7.4 monitoring fluorescence spectra upon excitation at 595 nm.

hexacation. Finally, it is worth noticing that the binding behavior in the presence of dsDNA is different from that in the presence of G4-DNA for both $[(PtCl_2)(CH_3)_6LZn]^{6+}$ and $[CH_3)_8LZn]^{8+}$.[5,20] Indeed, both compounds in the same experimental conditions as in the present study proved able to bind mainly as monomers to the parallel G-quadruplex structure. Apparently the smaller surface of the top and bottom base pairs as compared to that of a G-quartet is not favoring top and/or bottom binding in monomeric form.

Figure 6 shows the corrected fluorescence spectra for titration of $[(PtCl_2)(CH_3)_6LZn]^{6+}$ and $[CH_3)_8LZn]^{8+}$ with dsDNA. All of the solutions have absorbances lower than 0.1 at the excitation wavelength. The corrected excitation spectra measured at λ_{em} = 690 nm of $[(PtCl_2)(CH_3)_6LZn]^{6+}$ and $[(CH_3)_8LZn]^{8+}$ solutions are attributable to monomeric species, either free or complexed (Figures 2a,b, 5a,b). Inspection of Figure 6 shows a very important decrease of the emission intensity at high excess of porphyrazine over DNA, while a partial recovery of the intensity, accompanied by a ca. 10 nm red shift of λ_{max}, occurs on increasing the dsDNA concentration. These changes are consistent with negligible fluorescence from higher order DNA complexes (4:1 and 2:1). This is confirmed by singular value decomposition of the spectral data in Figure 6 indicating the presence of only two species with differentiated spectra, thereby supporting that free monomer and complexed monomer exclusively contribute to the total steady-state emission. Unfortunately, global fitting of the emission intensity titration data was not successful applying either the model used for absorption data or a different model. Thus, to achieve more insights into the nature of the fluorescent species in both systems, we also measured the fluorescence decay upon excitation at 373 nm in the absence and presence of various concentrations of dsDNA. The results are resumed in Table 1. The decay of the free ligands needs to be fitted with biexponential functions and exhibits one short-lived component of ca. $\tau_1 \approx 0.3–0.4$ ns, close to the resolution limit of the apparatus, and one long-lived component of $\tau_2 \approx 2.3–2.5$ ns. Considering that the product $a_i \times \tau_i$ is proportional to the intensity contribution of the i component in the steady-state spectrum at the observation wavelength, the long lifetime reasonably belongs to the monomeric species, while the short lifetime may be related to aggregated species negligibly contributing to the steady-state emission. For mixtures containing DNA at various concentrations, global analysis with a three exponential model afforded satisfactory results. A component with a markedly longer lifetime $\tau_3 \approx 8–9$ ns adds to

Table 1. Results for Global Analysis with a Triexponential Function of the Fluorescence Decays of 3×10^{-6} M Solution of $[(PtCl_2)(CH_3)_6LZn]^{6+}$ and $[(CH_3)_6LZn]^{8+}$ with Different Concentrations of dsDNA

	a_1	τ_1/ns	a_2	τ_2/ns	a_3	τ_3/ns
$[(PtCl_2)(CH_3)_6LZn]^{6+}$	0.030	0.33	0.053	2.34		
+ dsDNA, 1×10^{-6} M	0.12	0.32	0.023	2.20	0.001	8.90
+ dsDNA, 3×10^{-6} M	0.14	0.32	0.019	2.20	0.0015	8.90
+ dsDNA, 9×10^{-6} M	0.13	0.32	0.020	2.20	0.003	8.90
$[(CH_3)_6LZn]^{8+}$	0.010	0.37	0.056	2.52		
+ dsDNA, 1×10^{-6} M	0.078	0.42	0.029	2.30	0.002	7.71
+ dsDNA, 3×10^{-6} M	0.092	0.42	0.022	2.30	0.003	7.71
+ dsDNA, 9×10^{-6} M	0.085	0.42	0.023	2.30	0.005	7.71

two other components that are similar to those found in the free ligands. Considering that each pre-exponential factor is affected by the concentration of the respective emitting species, a positive correlation was found between a_3 and the concentration of the 1:1 complex, so that τ_3 can be reasonably assigned to this species. The pre-exponential factor a_1 of the short-lived component is strikingly dominant in the presence of DNA. Looking at the concentration profiles (Figure 5e and f), dimeric species, either free or complexed to DNA, clearly dominate over monomeric species. We therefore assign τ_1 to all kinds of dimeric species present in solution, free or complexed. We cannot distinguish their contribution in the steady-state spectra because their lifetimes are 10 times shorter and their quantum yield is likely much lower than those of monomeric species. No quantitative correlation with the concentration of the free monomer can be discerned for the pre-exponential factor a_2 of the intermediate lifetime component. The reason for this may be that we cannot unequivocally assign this lifetime to a single species, the free monomer, but monomeric species in higher order complexes may also contribute.

CD spectra of the $[(PtCl_2)(CH_3)_6LZn]^{6+}$ or $[(CH_3)_6LZn]^{8+}$ ligands in the presence of DNA in the UV region are represented in Figure 7a and b. The signal is typical for the B-form of dsDNA and, apart from intensity variations, does not undergo any significant change in shape at increasing DNA concentrations (see, for example, comparison of UV CD

dx.doi.org/10.1021/ic3020755 | Inorg. Chem. 2013, 52, 321–328

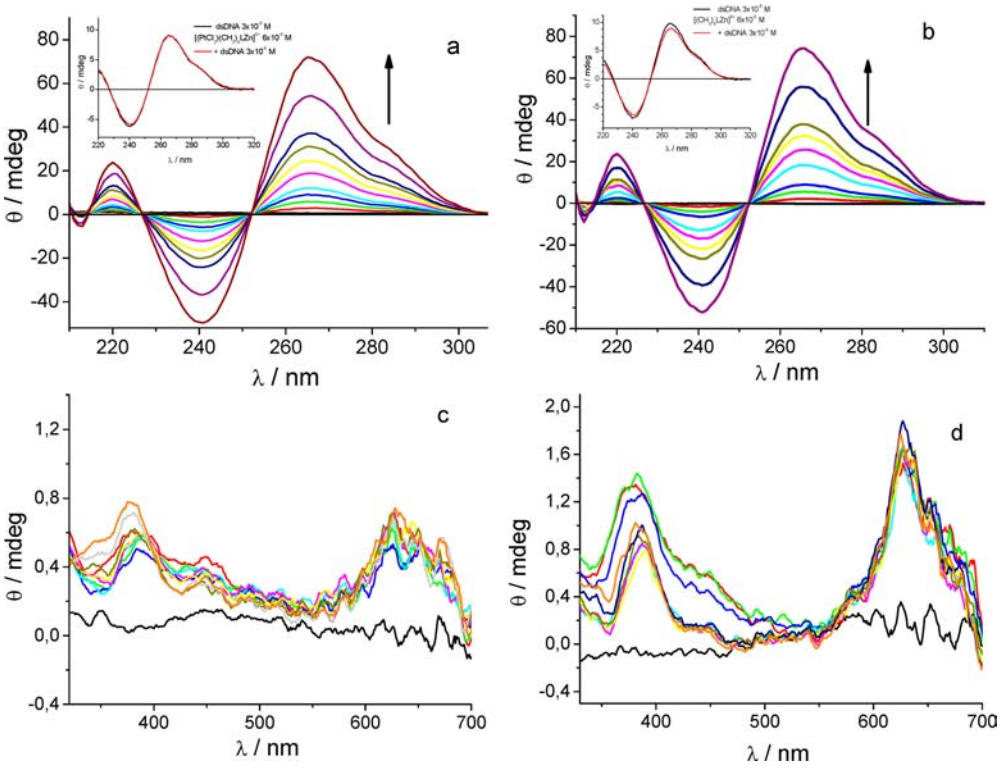

Figure 7. CD titration of a 6×10^{-6} M $[(PtCl_2)(CH_3)_6LZn]^{6+}$ (a,c) or $[(CH_3)_8LZn]^{8+}$ (b,d) solution with increasing dsDNA concentration (range $0.1-2.4) \times 10^{-5}$ M in Tris 10 mM buffer with KCl 0.1 M, pH 7.4, 22 °C. See Figure 1a,b for the color code. (a,b) UV circular dichroism spectra, d = 0.5 cm. Inset shows comparison of CD spectrum of 3×10^{-6} M dsDNA with and without macrocycle (c,d). Visible circular dichroism spectra, d = 2 cm. Spectra in (c) and (d) have been smoothed.

spectra of 3 μM dsDNA with and without macrocycle in the insets).[22] The similarity of all of the spectra indicates that the ligands do not intercalate, a binding mode expected to generate a strong increase of the CD of DNA in its duplex form.[23] This conclusion was also suggested by isothermal titration calorimetry (ITC) data, which revealed no heat exchange when a dsDNA solution was titrated with one of the two macrocycles. The macrocycles are not chiral themselves so we do not expect any CD signal for the monomeric species. The CD spectra in the absence of DNA corresponding to solutions with ca. 90% of either macrocycle present as dimer (black curve in Figure 7c and d) have very low intensity and do not evidence any exciton coupling between associated units. The weak induced CD signal in the 320–700 nm range relevant to the porphyrazine electronic transitions confirms that complexation to dsDNA occurs but does not exhibit any clear-cut negative band, further supporting that these molecules do not intercalate (Figure 7c,d). Indeed, negative signals in this spectral region have been assigned to intercalation in the case of porphyrine–DNA binding.[24,25] Furthermore, no clear bisignate band is observed, so exciton coupling between two ligands is negligible when more than one porphyrazine macrocycle associates to DNA.[24]

■ CONCLUSIONS

The noncovalent binding of $[(PtCl_2)(CH_3)_6LZn]^{6+}$ to dsDNA was compared to that of $[(CH_3)_8LZn]^{8+}$. From analysis of UV–vis absorption data, we obtained as the most reliable complexation model for both molecules the one comprising associates of one dsDNA molecule with 1, 2, and 4 macrocycles. The analysis was supported by DFT/TDDFT calculations affording the ground-state molecular and electronic structure as well as the absorption spectrum for the optimized geometry of the $[(PtCl_2)(CH_3)_6LZn]^{6+}$ derivative. The excitation energies and oscillator strengths calculated for the singlet excited states of the hexacation up to 450 nm were in excellent agreement with spectroscopic data obtained in the presence of SDS micelles.

The present study evidenced that the *cis*-platin functionality positively influences the behavior of $[(PtCl_2)(CH_3)_6LZn]^{6+}$ in the frame of a potential, multimodal therapeutic approach. A more marked monomerization of $[(PtCl_2)(CH_3)_6LZn]^{6+}$ versus $[(CH_3)_8LZn]^{8+}$ on binding to dsDNA was assessed. This fact is expected to improve the photochemical behavior of the sensitizer. Both generation of singlet oxygen and other photochemical processes can become feasible. A further possible outcome is covalent binding of the *cis*-platin unit to DNA. The process is known to occur thermally for *cis*-platin derivatives and involve one or two dG residues. Crystal structures of dsDNA complexes with *cis*-platin compounds show that Pt(II) mainly binds to N(7) of guanine, not engaged in any hydrogen bonding when forming the Watson–Crick base pair with cytosine.[26] The higher degree of monomerization observed for $[(PtCl_2)(CH_3)_6LZn]^{6+}$ in the dsDNA complexes may represent a favorable condition for the establishment of a covalent bond. Differently, N(7) is involved in hydrogen bonding in the Hoogsteen motif for the formation of the planes of four guanines in G4-DNA and consequently may be not accessible for platinum binding to the G4 structure. Consistently, no important differences were observed[5,20] between $[(PtCl_2)(CH_3)_6LZn]^{6+}$ and $[(CH_3)_8LZn]^{8+}$ in the binding to G4-DNA.

dx.doi.org/10.1021/ic3020755 | *Inorg. Chem.* 2013, 52, 321–328

■ ASSOCIATED CONTENT

Supporting Information

Aggregation details, global analysis, and Cartesian coordinates. This material is available free of charge via the Internet at http://pubs.acs.org.

■ AUTHOR INFORMATION

Corresponding Author

*E-mail: ilse.manet@isof.cnr.it.

Notes

The authors declare no competing financial interest.

■ ACKNOWLEDGMENTS

We thank Dr. B. Zambelli of the University of Bologna for the ITC measurements. M.P.D. is grateful to Prof. F. Monacelli (University of Rome) for useful discussions and the CIRCMSB (Consorzio Interuniversitario di Ricerca in Chimica dei Metalli nei Sistemi Biologici) for scientific support.

■ REFERENCES

(1) Crescenzi, E.; Chiaviello, A.; Canti, G.; Reddi, E.; Veneziani, B. M.; Palumbo, G. *Mol. Cancer Ther.* **2006**, *5*, 776−785. Faivre, S.; Le Chevalier, T.; Monnerat, C.; Lokiec, R.; Novello, S.; Taieb, J.; Pautier, P.; Lhomme, C.; Ruffie, P.; Kayitalire, L.; Armand, J. P.; Raymond, E. *Ann. Oncol.* **2002**, *13*, 1479−1489.

(2) Sortino, S. *J. Mater. Chem.* **2012**, *22*, 301−318. Kralova, J.; Kejik, Z.; Briza, T.; Pouckova, P.; Kral, A.; Martasek, P.; Kral, V. *J. Med. Chem.* **2010**, *53*, 128−138. Lottner, C.; Knuechel, R.; Bernhardt, G.; Brunner, H. *Cancer Lett.* **2004**, *215*, 167−177. Lottner, C.; Knuechel, R.; Bernhardt, G.; Brunner, H. *Cancer Lett.* **2004**, *203*, 171−180. Nemykin, V. N.; Mytsyk, V. M.; Volkov, S. V.; Kobayashi, N. *J. Porphyrins Phthalocyanines* **2000**, *4*, 551−554.

(3) Donzello, M. P.; Vittori, D.; Viola, E.; Manet, I.; Mannina, L.; Cellai, L.; Monti, S.; Ercolani, C. *Inorg. Chem.* **2011**, *50*, 7391−7402.

(4) Ethirajan, M.; Chen, Y. H.; Joshi, P.; Pandey, R. K. *Chem. Soc. Rev.* **2011**, *40*, 340−362.

(5) Manet, I.; Manoli, F.; Donzello, M. P.; Ercolani, C.; Vittori, D.; Cellai, L.; Masi, A.; Monti, S. *Inorg. Chem.* **2011**, *50*, 7403−7411.

(6) Balasubramanian, S.; Neidle, S. *Curr. Opin. Chem. Biol.* **2009**, *13*, 345−353. Qin, Y.; Hurley, L. H. *Biochimie* **2008**, *90*, 1149−1171. Harley, C. B. *Nat. Rev. Cancer* **2008**, *8*, 167−179. De Cian, A.; Lacroix, L.; Douarre, C.; Temime-Smaali, N.; Trentesaux, C.; Riou, J. F.; Mergny, J. L. *Biochimie* **2008**, *90*, 131−155. Shi, D. F.; Wheelhouse, R. T.; Sun, D. Y.; Hurley, L. H. *J. Med. Chem.* **2001**, *44*, 4509−4523. Hurley, L. H. *Biochem. Soc. Trans.* **2001**, *29*, 692−696.

(7) Ou, T. M.; Lu, Y. J.; Tan, J. H.; Huang, Z. S.; Wong, K. Y.; Gu, L. Q. *ChemMedChem* **2008**, *3*, 690−713.

(8) Luedtke, N. W. *Chimia* **2009**, *63*, 134−139.

(9) Kelland, L. *Nat. Rev. Cancer* **2007**, *7*, 573−584. Raymond, E.; Faivre, S.; Chaney, S.; Woynarowski, J.; Cvitkovic, E. *Mol. Cancer Ther.* **2002**, *1*, 227−235.

(10) Bergami, C.; Donzello, M. P.; Monacelli, F.; Ercolani, C.; Kadish, K. M. *Inorg. Chem.* **2005**, *44*, 9862−9873.

(11) *ADF 2012.01*; SCM, Theoretical Chemistry, Vrije Universiteit: Amsterdam, The Netherlands, available from http://www.scm.com.

(12) te Velde, G.; Bickelhaupt, F. M.; Baerends, E. J.; Fonseca Guerra, C.; Van Gisbergen, S. J. A.; Snijders, J. G.; Ziegler, T. *J. Comput. Chem.* **2001**, *22*, 931−967. Fonseca Guerra, C.; Snijders, J. G.; te Velde, G.; Baerends, E. J. *Theor. Chem. Acc.* **1998**, *99*, 391−403. Baerends, E. J.; Ellis, D. E.; Ros, P. *Chem. Phys.* **1973**, *2*, 41.

(13) van Lenthe, E.; Ehlers, A.; Baerends, E. J. *J. Chem. Phys.* **1999**, *110*, 8943−8953. van Lenthe, E.; Baerends, E. J.; Snijders, J. G. *J. Chem. Phys.* **1994**, *101*, 9783−9792. van Lenthe, E.; Baerends, E. J.; Snijders, J. G. *J. Chem. Phys.* **1993**, *99*, 4597−4610.

(14) van Lenthe, E.; Baerends, E. J. *J. Comput. Chem.* **2003**, *24*, 1142−1156.

(15) Becke, A. D. *J. Chem. Phys.* **1988**, *88*, 1053−1062. Perdew, J. P.; Yue, W. *Phys. Rev. B* **1986**, *33*, 8800−8802.

(16) Becke, A. D. *J. Chem. Phys.* **1993**, *98*, 5648−5652. Lee, C. T.; Yang, W. T.; Parr, R. G. *Phys. Rev. B* **1988**, *37*, 785−789.

(17) Pye, C. C.; Ziegler, T. *Theor. Chem. Acc.* **1999**, *101*, 396−408. Klamt, A.; Jonas, V. *J. Chem. Phys.* **1996**, *105*, 9972−9981. Klamt, A. *J. Phys. Chem.* **1995**, *99*, 2224−2235. Klamt, A.; Schuurmann, G. *J. Chem. Soc., Perkin Trans. 2* **1993**, 799−805.

(18) Scalmani, G.; Frisch, M. J.; Mennucci, B.; Tomasi, J.; Cammi, R.; Barone, V. *J. Chem. Phys.* **2006**, 124. Klamt, A. *J. Phys. Chem.* **1996**, *100*, 3349−3353.

(19) Gray, R. D.; Li, J.; Chaires, J. B. *J. Phys. Chem. B* **2009**, *113*, 2676−2683.

(20) Manet, I.; Manoli, F.; Donzello, M. P.; Viola, E.; Andreano, G.; Masi, A.; Cellai, L.; Monti, S. *Org. Biomol. Chem.* **2011**, *9*, 684−688.

(21) Cai, X. H.; Donzello, M. P.; Viola, E.; Rizzoli, C.; Ercolani, C.; Kadish, K. M. *Inorg. Chem.* **2009**, *48*, 7086−7098.

(22) Ranjbar, B.; Gill, P. *Chem. Biol. Drug Des.* **2009**, *74*, 101−120. Kypr, J.; Kejnovska, I.; Renciuk, D.; Vorlickova, M. *Nucleic Acids Res.* **2009**, *37*, 1713−1725.

(23) Saha, I.; Hossain, M.; Kumar, G. S. *Phys. Chem. Chem. Phys.* **2010**, *12*, 12771−12779. Saha, I.; Hossain, M.; Kumar, G. S. *J. Phys. Chem. B* **2010**, *114*, 15278−15287. Garbett, N. C.; Ragazzon, P. A.; Chaires, J. B. *Nat. Protoc.* **2007**, *2*, 3166−3172.

(24) Balaz, M.; Bitsch-Jensen, K.; Mammana, A.; Ellestad, G. A.; Nakanishi, K.; Berova, N. *Pure Appl. Chem.* **2007**, *79*, 801−809.

(25) Pasternack, R. F. *Chirality* **2003**, *15*, 329−332.

(26) Lovejoy, K. S.; Todd, R. C.; Zhang, S. Z.; McCormick, M. S.; D'Aquino, J. A.; Reardon, J. T.; Sancar, A.; Giacomini, K. M.; Lippard, S. J. *Proc. Natl. Acad. Sci. U.S.A.* **2008**, *105*, 8902−8907. Silverman, A. P.; Bu, W. M.; Cohen, S. M.; Lippard, S. J. *J. Biol. Chem.* **2002**, *277*, 49743−49749.